Buried thermoplastic layer diagnostics by the use of combined frequency-domain and impulse response photo-thermo-mechanical radiometry

Mahendra Munidasa[a] and Andreas Mandelis
Photothermal and Optoelectronic Diagnostics Laboratories, Department of Mechanical and Industrial Engineering, University of Toronto and Manufacturing Corporation of Ontario, 5 King's College Road, Toronto, Ontario, Canada M5S 3G8

Mel Ball
Alcan International Ltd., Research & Development Center, Box 8400, Kingston, Ontario, Canada K7L 5L9

(Received 29 August 1997; accepted for publication 30 October 1997)

A photothermal approach to the problem of characterizing the thermoplastic layer thickness sandwiched between two metal foils used in heat-sealed food containers is described. Real-time signal acquisition instrumentation for the photothermal radiometric signal based on impulse-response fast Fourier transform (FFT) processing via chirped laser-beam modulation and cross-correlation spectral analysis, instead of the conventional point-by-point discrete frequency scans with a lock-in amplifier has been introduced. A theoretical frequency-domain model for the signal generation due to laser heating, which contains both a thermal component and a mechanical component due to the thermal expansion of the thermoplastic layer, is presented. The time domain impulse response theoretical data have been obtained by a numerical FFT of the frequency-domain theoretical data. The total signal was measured via radiometric detection in both domains and was fitted to the theory to obtain thermal transport properties of the three-layered system. The thickness of the thermoplastic layer has been extracted with better than 5% precision. © *1998 American Institute of Physics.* [S0034-6748(98)01102-2]

I. INTRODUCTION

Nondestructive evaluation of buried layers finds important applications in industry. In this article we describe a fast, noncontact photothermal technique for thermomechanical characterization of a thermoplastic layer sandwiched between two metal foils used in heat-sealed food containers. For this particular application a noncontact measurement was required of the thickness of the polymer layer between two layers of aluminum in a heat-sealed container rim at a speed of four locations of the container in 60 s.

Photothermal techniques involve launching a thermal wave in the sample through laser excitation and detection of the resulting temperature at an external boundary of the sample. Photothermal excitation and acquisition of thermal wave information may be achieved via several measurement approaches, including (a) single-frequency harmonic excitation using a sinusoidally modulated cw laser source and lock-in detection of the frequency dependent temperature,[1] (b) pulsed excitation and observation of the transient signal,[2] (c) broadband-modulation cw excitation (fast linear frequency sweep chirp) with simultaneous detection of the whole frequency response spectrum and fast Fourier transform (FFT) to obtain impulse response.[3] Single-frequency cw harmonic excitation is performed on a point-by-point basis and has a good signal-to-noise ratio (SNR) but cannot be done in real time. On the other hand the disadvantage of pulsed excitation is that it delivers high peak power, which results in low damage threshold for many materials. Furthermore, chirped excitation is characterized by the low incident power density and high source stability inherent in cw laser systems. It also has the advantage of high speed data acquisition compared with point-by-point single frequency measurements.

For complex sample geometries the thermal-wave measurement of specific parameters (such as thicknesses or thermophysical properties of multilayered solids) may be ill defined, in the sense that several parameter sets may result in identical signals. The combination of frequency domain and time domain signal methodologies described in this work has helped towards the unique identification of buried layer thickness and thermal properties of all the layers. Data from both methods (a) and (c) are presented which helped to understand the signal generation mechanism and deconvolute the various parameter contributions. Method (c) is the one to be used for actual online measurements.

II. EXPERIMENT

Figure 1 shows the schematic of the experimental setup used in the laboratory. An intensity modulated Ar-ion laser (500 mW) is focused on to one surface of the layered structure and the temperature on the opposite surface is monitored (heat-sealed rim of the food container was accessible from both sides) via infrared radiometric detection[4] using two paraboloidal mirrors and a liquid-nitrogen cooled HgCdTe ir detector. For the point-by-point frequency scan method, the internal oscillator of the lock-in amplifier is used to drive an acousto-optic modulator which modulates the laser beam in-

[a]Current address: Valmet Automation (Canada) Ltd., 111 Granton Dr., Richmond Hill, ON Canada L4B 1L5.

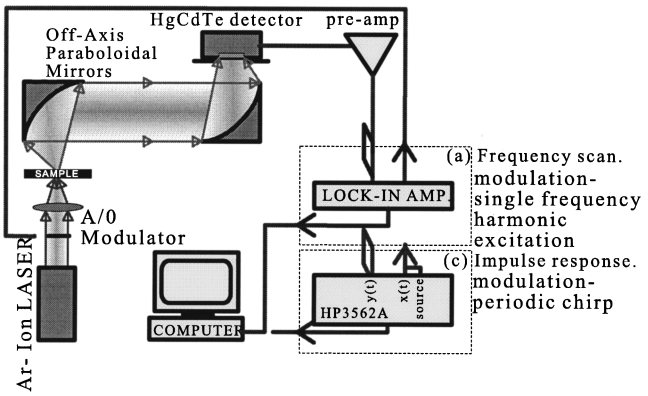

FIG. 1. Schematic of the experimental setup.

tensity. The signal from the detector is preamplified and sent to the lock-in amplifier. The lock-in is interfaced to the computer for automated data acquisition. For the chirped excitation method the central excitation/detection component in the system is an analyzer (HP3562A) equipped with an internal frequency synthesizer. The synthesizer is capable of generating linear frequency sweeps (chirp) with a modulation bandwidth up to 100 kHz. The sweep source is used to drive the acousto-optic modulator. The impulse response averaged over several chirp cycles recorded on the FFT analyzer is saved into a personal computer.

III. THEORY

A. Thermal-wave field

Solving the heat diffusion equation for the system shown in Fig. 2, assuming continuity of temperature field and the derivative of the field, evaluating the temperature at $x=L_1+L_2+L_3$ in a one-dimensional geometry (Fig. 2) one obtains [5]

$$\Theta(L_1+L_2+L_3,\omega)=\frac{F_0}{k_1\sigma_1}\frac{2(1+R_1)e^{-\sigma_1 L_1}}{Z_2-R_1Z_1e^{-2\sigma_1 L_1}}\times(1+R_3)e^{-\sigma_3 L_3}.$$

The above equation can be recast in a three-dimensional formalism taking into account the Gaussian lateral intensity profile of the laser beam by use of a Hankel transformation[6] (at the center of the laser spot)

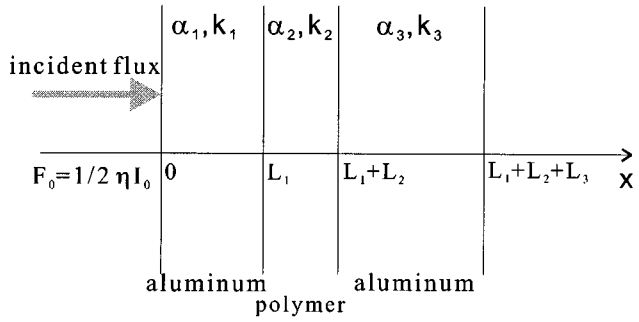

FIG. 2. Layered structure of the sample under investigation.

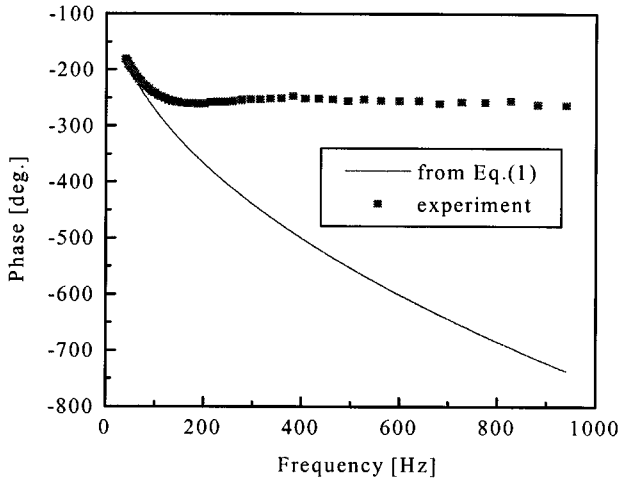

FIG. 3. Phase of the photothermal frequency scan data from one of the samples with the structure shown in Fig. 2 and the theoretically calculated photothermal signal phase from Eq. (1).

$$T(L_1+L_2+L_3,\omega)=F_0\int_0^\infty\frac{1}{k_1\sigma_1}\frac{2(1+R_1)e^{-\sigma_1 L_1}}{Z_2-R_1Z_1e^{-2\sigma_1 L_1}}\times(1+R_3)e^{-\sigma_3 L_3}e^{-\lambda^2 r^2/8}J_1(a\lambda)d\lambda, \quad (1)$$

where
$\sigma_j^2=\lambda^2+i\omega/\alpha_j;\ j=1,2,3,$
ω=angular modulation frequency of laser intensity,
a=radius of the detector,
r=radius of the laser beam spot,
$\alpha_1=\alpha_3=\alpha_{\mathrm{Al}}$=thermal diffusivity of aluminum,
$k_1=k_3=k_{\mathrm{Al}}$=thermal conductivity of aluminum,
$\alpha_2=\alpha_{\mathrm{pol}}$=thermal diffusivity of the polymer,
$k_2=k_{\mathrm{pol}}$=thermal conductivity of the polymer,
$L_2=L_{\mathrm{pol}}$=thickness of the polymer,
$b_{ij}=k_i\sigma_i/k_j\sigma_j$,
$R_1=R_3=R=(b_{10}-1)/(b_{10}+1)\cong 1$; ''0'' refers to air,
$Z_1=(1+b_{21})X_{32}\exp(-\sigma_2 L_2)+(1-b_{21})Y_{32}\exp(\sigma_2 L_2)$,
$Z_2=(1-b_{21})X_{32}\exp(-\sigma_2 L_2)+(1+b_{21})Y_{32}\exp(\sigma_2 L_2)$,
$X_{32}=(1-b_{32})+R_3(1+b_{32})\exp(-2\sigma_3 L_3)$,
$Y_{32}=(1+b_{32})+R_3(1-b_{32})\exp(-2\sigma_3 L_3)$, and
J_1=first order Bessel function of the first kind.

Figure 3 shows the experimental phase data from one of the samples and the theoretical calculation from Eq. (1) using the measured thicknesses, and material properties found in the literature. This shows a great discrepancy at higher frequencies confirming that pure heat diffusion is not the only signal generating mechanism. Observation of a signal several thermal diffusion lengths away from the laser spot led us to believe that there is a mechanical component detected by the ir detector. This is most probably due to the thermal expansion of the polymer which moves the aluminum layer in and out of focus of the detection optics.

B. Photo-thermo-elastic theory of three-layer structure

In deriving an expression for the displacement of the sample surface the following assumptions have been made.

An unconstrained expansion of the polymer due to the laser-induced thermal-wave field is assumed. Also, the displacement at $x=L_1+L_2$ is assumed to be rigidly manifested as an equal displacement at $x=L_1+L_2+L_3$, i.e., only the polymer expanded during the optical heating cycle. Initially a one-dimensional expression will be derived and then it will be extended to a three-dimensional expression.

In the presence of both heating and actual stress, the stress–strain relation in the polymer can be written as[7]

$$\Delta p(x;\omega)=(\lambda^*+2\mu^*)\epsilon(x;\omega)-B\alpha_t\Delta\theta(x;\omega) \tag{2a}$$

with unconstrained boundary conditions

$$\Delta p(L_1;\omega)=\Delta p(L_1+L_2;\omega)=0, \tag{2b}$$

where the following definitions were made:

λ^*: Lamé constant — μ^*: modulus of strain
$\epsilon(x;\omega)$: modulated strain — $\Delta p(x;\omega)$: modulated stress
$\Delta\theta(x;\omega)$: thermal-wave intensity — B: bulk modulus
α_t: coefficient of linear thermal expansion.

Using

$$\epsilon(x:\omega)=\frac{\partial}{\partial x}\Delta U(x,\omega t),$$

the displacement as a result of harmonic thermal expansion,

$$\Delta U(x,\omega t)=\Delta u(x)e^{i\omega t},$$

and the equation of motion of an elastic wave in the solid

$$\rho\frac{\partial^2}{\partial t^2}\Delta U(x,\omega t)=\frac{\partial}{\partial x}\Delta p(x;\omega),$$

with Eq. (2), we obtain

$$\frac{d^2}{dx^2}\Delta u(x;\omega)+k^2\Delta u(x;\omega)=\alpha_t\frac{d}{dx}\Delta\theta(x;\omega),$$

$$L_1\leqslant x\leqslant L_1+L_2, \tag{3}$$

where $k=\omega/c_0$ and $c_0=$speed of sound in the polymer.

The spatial thermal-wave profile in the polymer is given by

$$\Delta\theta(x;\omega)\equiv T_{\rm pol}(x;\omega)=\frac{\alpha_{\rm pol}}{2k_{\rm pol}}I_0\left(\frac{1+R}{\alpha_{\rm Al}\sigma_1}\right)\frac{e^{-\sigma_1L_1}}{Z_2-RZ_1e^{-2\sigma_1L_1}}\times[X_{32}e^{-\sigma_2(L_1+L_2-x)}+Y_{32}e^{\sigma_2(L_1+L_2-x)}]. \tag{4}$$

Combining Eqs. (3) and (4), and the unconstrained boundary conditions (2b), and then extending the formalism to three dimensions, the displacement at the center of the laser spot is given by the Hankel integral[6]

$$\Delta u(L_1+L_2+L_3,\omega)=\int_0^\infty\frac{\alpha_t}{k^2+\sigma_2^2}\{E(\omega)[k(\csc kL_2-e^{\sigma_2L_2}\cot kL_2)+\sigma_2e^{\sigma_2L_2}]e^{\sigma_2L_1}+V(\omega)[k(\csc kL_2-e^{-\sigma_2L_2}\cot kL_2)-\sigma_2e^{-\sigma_2L_2}]e^{-\sigma_2L_1}\}\times J_1(a\lambda)e^{-\lambda^2r^2/8}d\lambda, \tag{5}$$

where

$$E(\omega)=\left(\frac{I_0\alpha_2X_{32}}{2k_2\alpha_1\sigma_1Z_2}\right)\frac{(1+R)e^{-\sigma_1L_1-\sigma_2(L_1+L_2)}}{1-R\rho e^{-2\sigma_1L_1}},$$

$$V(\omega)=\left(\frac{I_0\alpha_2Y_{32}}{2k_2\alpha_1\sigma_1Z_2}\right)\frac{(1+R)e^{-\sigma_1L_1+\sigma_2(L_1+L_2)}}{1-R\rho e^{-2\sigma_1L_1}},$$

and ρ is the ratio z_1/z_2.

The total photothermal radiometric (PTR) signal detected by the ir detector is a combination of the thermal-wave temperature field given by Eq. (1) and the mechanical component due to the periodic expansion of the strip surface, going in and out of focus of the detection optics as given by Eq. (5). Therefore, the total PTR signal can be written compactly as

$$S_{\rm PTR}(L_1+L_2+L_3,\omega)=s_1\times T(L_1+L_2+L_3,\omega)+s_2\times\Delta u(L_1+L_2+L_3,\omega), \tag{6}$$

where s_1 and s_2 determine the contribution from each component. These two parameters can be reduced to a single parameter s, plus an arbitrary normalization constant. The normalization constant does not play a role in determining the phase of the signal. The parameter s is one of the parameters to be determined through multiparameter fit discussed in the next section. The value of s only determines the percentage of the mechanical component that has to be added to the thermal component, to correctly predict the experimental data, and it has no other physical significance such as the values of material parameters presented in the next section. The results in the next section will show that Eq. (6) correctly predicts the experimental data.

The theoretical photo-thermo-mechanical impulse response was obtained by a FFT of the numerical data calculated from Eq. (6). We used Microcal Origin 4.1 software[8] to perform the FFT.

IV. RESULTS

Results from two samples with different polymer thicknesses are presented here. In both samples the aluminum foil thickness on the laser irradiated side was 70 μm and that on the opposite side was 110 μm. The total thickness of the heat seal was measured with a micrometer and the aluminum foil thickness was subtracted to obtain the polymer thickness. For sample No. 1 the polymer thickness was 50 ± 5 μm and for sample No. 2 it was 40 ± 5 μm. The laser spot size was measured to be 15 μm.

Data from both frequency scan and impulse response were used for self-consistent fitting. The signal is insensitive to the mechanical properties of the layered structure. It is sensitive however, to the thermal parameters, thicknesses,

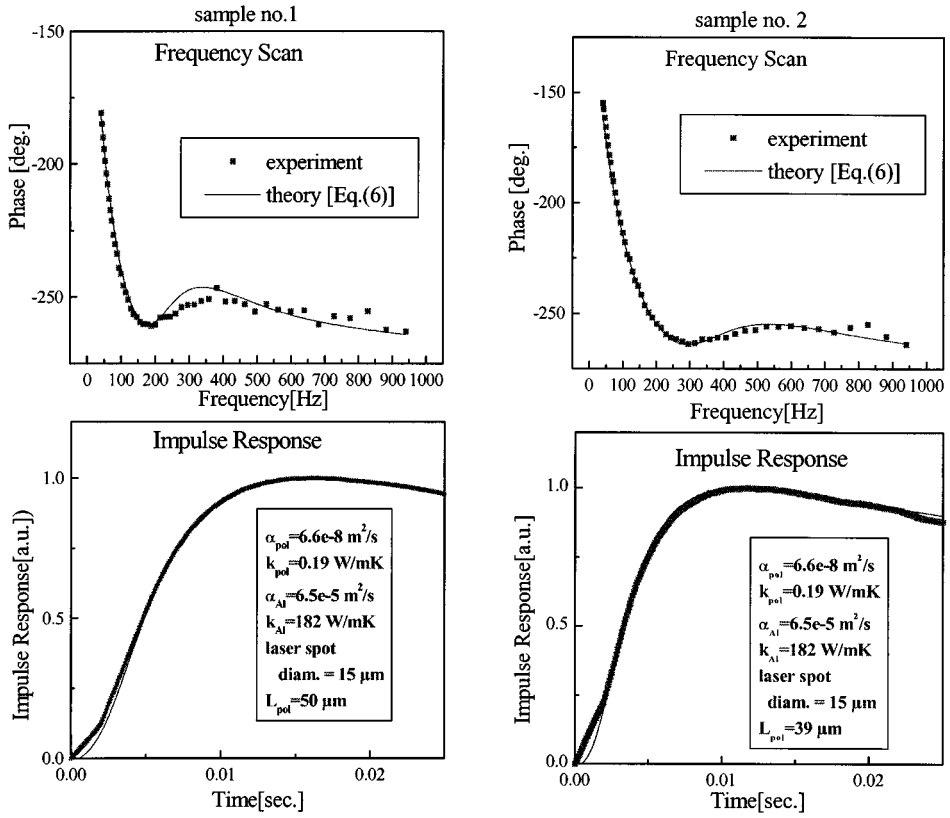

FIG. 4. Experimental frequency scan phase data, impulse response data, and the corresponding theoretical fit for two samples with different buried thermoplastic layer thicknesses. Values of the fitted parameters are shown in the insets.

and the coupling parameter s [see definition below Eq. (6)]. Each parameter (or a set of parameters) is sensitive to different features of the signal such as the phase minimum, the high frequency value of the phase, the impulse response peak time, the rise time, and the decay rate. Since the amplitude of the frequency scan was featureless it was not used. Fitting data in both domains, one after the other, helps to uniquely determine all the parameters.

Figure 4 shows the experimental data and the corresponding theoretical fits together with the fitted parameters for both frequency scan phase and impulse response. Sample No. 1 data (both frequency domain and time domain) were fitted first using the measured thickness (50 μm). Then the same fitting parameters except the thickness of the polymer were used to fit sample No. 2 which gave a thickness of 39 μm for that sample. This value is in agreement with the independently measured thickness value of 40 ± 55 μm.

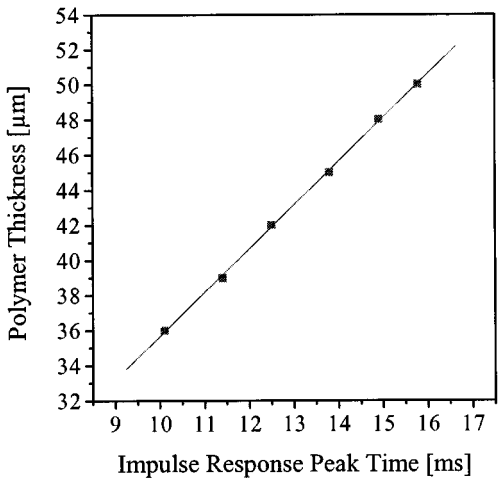

FIG. 5. The relationship between the impulse response peak time and the polymer thickness.

V. DISCUSSION

The theory shows that a linear relationship exists between the polymer thickness and the impulse response peak time which makes it easier to calibrate a given nondestructive evaluation signal-generating process as shown in Fig. 5. The fitting parameters for a given process can be found using both frequency-domain and time-domain data as shown above. Then using only the impulse response data, in each measurement the peak of the response can be monitored and the polymer thickness can be read from the calibration curve. The impulse response data (Fig. 4) collection time was 10 s (1024 points) at 5 kHz bandwidth, averaged over 20 chirp cycles, and adjacent average smoothing. Therefore, the total time for making one thickness measurement is about 15 s. The frequency scan data collection time with 1 s lock-in time constant was about 20 min. Precision of peak time measurement for the data shown is 0.5 ms. From the calibration

curve this translates into polymer thickness precision of ± 1 μm ($\pm 2.5\%$ at 40 μm). Since the SNR increases as the polymer thickness decreases, precision could be better than 5% even for thinner polymer thicknesses.

In conclusion, it has been shown that the combination of frequency-domain and time-domain impulse response photothermal signals can be used successfully to measure the thickness of a buried layer by allowing the determination of several material parameters (conductivity and diffusivity of the metallic foil overlayer). Without the frequency-domain and time-domain combination, the unique identification and measurement of the proper set of parameters of the composite structure would not be possible.

ACKNOWLEDGMENTS

The support of the Manufacturing Research Corporation of Ontario (MRCO) and Alcan International Ltd. is gratefully acknowledged.

[1] J. Opsal and A. Rosencwaig, J. Appl. Phys. **53**, 4240 (1982).
[2] L. C. Aamodt, J. W. Maclachlan Spicer, and J. C. Murphy, J. Appl. Phys. **68**, 6087 (1990).
[3] J. F. Power and A. Mandelis, Rev. Sci. Instrum. **58**, 2024 (1987).
[4] S. O. Kanstad and P. E. Nordal, Can. J. Phys. **64**, 1155 (1986).
[5] A. Mandelis (unpublished).
[6] A. Mandelis and J. F. Power, Appl. Opt. **27**, 3408 (1988).
[7] R. M. White, J. Appl. Phys. **34**, 3559 (1963); A. Rosencwaig, *Photoacoustics and Photoacoustic Spectroscopy* (Wiley, New York, 1980), pp. 115–123.
[8] Microcal Software, Inc., Northampton, MA 01060.